Volume 1 | Number 1 | Jan 2013 | Pages 1–100

ChemComm

Chemical Communications
www.rsc.org/chemcomm

ROYAL SOCIETY OF CHEMISTRY

This is an *Accepted Manuscript*, which has been through the Royal Society of Chemistry peer review process and has been accepted for publication.

Accepted Manuscripts are published online shortly after acceptance, before technical editing, formatting and proof reading. Using this free service, authors can make their results available to the community, in citable form, before we publish the edited article. We will replace this *Accepted Manuscript* with the edited and formatted *Advance Article* as soon as it is available.

You can find more information about *Accepted Manuscripts* in the **Information for Authors**.

Please note that technical editing may introduce minor changes to the text and/or graphics, which may alter content. The journal's standard **Terms & Conditions** and the **Ethical guidelines** still apply. In no event shall the Royal Society of Chemistry be held responsible for any errors or omissions in this *Accepted Manuscript* or any consequences arising from the use of any information it contains.

www.rsc.org/chemcomm

Journal Name

COMMUNICATION

Fabrication of Highly-specific SERS Substrates by Co-precipitation of Functional Nanomaterials during the Self-sedimentation of Silver Nanowires into Nanoporous Film

Rui Liu,[a] Jie-fang Sun,[a] Dong Cao,[a] Li-qiang Zhang,[b] Jing-fu Liu[a] and Gui-bin Jiang[a]

In this report, we propose and demonstrate the fabrication of a highly-specific surface enhanced Raman scattering (SERS) substrate, which was achieved by co-precipitation of functional materials such as nanosorbent and nanocatalyst into Ag nanoporous films. Based on the developed nanostructures, we performed ultrasensitive detection of arsenic ion by SERS and monitored catalyzed reactions by real-time SERS.

Since its discovery in the 1970s,[1] surface enhanced Raman scattering (SERS) has been a research topic of continual interest. Relative to other spectroscopic tools, SERS is novel due to its single-molecule fingerprint spectra provision aptness,[2] minimal sample preparation requirements, ease of operation, high tolerance for aqueous samples, and greater adaptability compared to other methods. As a result, SERS has been widely applied in various fields that range from *in situ* investigation of catalytic reactions[3] to *in vivo* studies of biological processes at the single-cell level.[4] Since the SERS phenomenon primarily occurs on the near-field of a SERS substrate, integrating the system of interest with a SERS substrate is of central importance. In simple cases, SERS can be used to observe probe molecules with well-defined morphology[5], or hierarchical ensembles of probe molecules with precisely designed configurations, when they are directly anchored to nano objectives (as SERS substrates) made from plasmonic noble metals (Au, Ag, Cu).[6] In other occasions, especially in the use of SERS to study chemical or biological processes, conferring the target with SERS activity is much more complicated, though this can be partially achieved *via in-situ* generated Au/Ag particles,[4e] or by borrowing SERS activity from an implanted substrate.[3c, 3d] One strategy for the use of SERS is to design what we term a "task-specific SERS substrate," that is, a SERS substrate designed with specific functionality to achieve a desired task. However, the uneven and imprecise implantation of other materials into SERS hotspots, where the majority of SERS is generated,[7] makes this strategy less effective. The only successful example of this approach is a report where Au or Ag nanoparticles (NPs) were anchored on Graphene oxide (GO) or reduced GO (rGO) to capture an analyte with low affinity for Au or Ag.[8] Although ultrasensitive detection was achieved for the target molecule, the Raman signal of GO/rGO was slightly enhanced.[8c]

One solution to this problem is to fabricate three-dimensional (3D) Au or Ag nanoporous films (NPF) as SERS substrates using a bottom-up approach.[6d] The abundant nanopores within NPFs are highly SERSactive due to their ability to couple the electromagnetic field between ligaments effectively.[6f] Moreover, these nanopores are ready to accommodate new materials and confer them with SERS activity. Additionally, the bottom-up method of the NPF fabrication process allows the doped material in a hybrid NPF to be evenly distributed. Herein, we report the first example of template-free fabrication of Ag NPF from the self-organization of Ag nanowires (NWs).[6d] As a proof-of-concept, nanosorbent (γ-Fe_2O_3 nanosheets (NSs)) or nanocatalyst (Pd overlayer/branches) was co-precipitated into the Ag NPF. In addition to describing a new route for the fabrication of SERS-active Ag NPF, we developed a group of "task-specific SERS substrates." In these fabricated hybrid NPFs, the Ag surface was selectively blocked while its SERS activity was well-preserved. This method effectively enhanced the Raman signal of adsorbed arsenic/arsenite ions (As(III)/As(V)) and facilitated the real-time monitoring of catalyzed reactions.

Physical characterization of the developed nanostructures is presented in Fig. 1, and the experimental for their fabrication are provided in electronic supporting information (ESI). Interconnected Ag NWs with diameters of 20-30 nm were prepared using a protocol adapted from our previous work (Fig. 1A).[9] Compared with similarly prepared Au, Pd, or Pt NWs, the morphology of the Ag NWs was less uniform, which we ascribe to the weaker π-d interaction between Ag and the stabilizer Triton X-114. After self-organization/sedimentation on any substrate, namely, Si wafer or SiO_2 slide, sub-centimeter sized crack-free Ag NPF were fabricated. The Ag NPF had a thickness of about 3 µm and consisted of uniform ligaments and nanochannels in the range of 30-50 nm (Fig. 1B, with an average diameter of 36.09±12.48 nm, and S1). Further analysis showed that Ag is in its metallic form, with Ag 3d electrons located at 368.2 and 374.2 eV (XPS spectra in Fig. 1 C1). The XRD pattern revealed that the Ag NPF possessed a face-centered cubic structure, which is in good agreement with ICDD card data. Moreover, based on Scherrer line broadening analysis, the size of the ligaments was ~32 nm, which is consistent with FESEM inspection (Fig. C2). The UV-vis extinction spectra of Ag NWs showed two pronounced peaks at ~340 and ~385 nm (Fig. C3). The shoulder around 340 nm (marked by the red arrow) was attributed to the plasmon resonance

of bulk silver, which results from the network character of Ag NWs.[6b] The broad peak around 385 nm and the extinction at above 500 nm are presumably attributed to the transverse plasmon band and the longitudinal plasmon band of Ag NWs, respectively. However, for the further interconnection of NWs, no significant peak was identified in the Ag NPF.
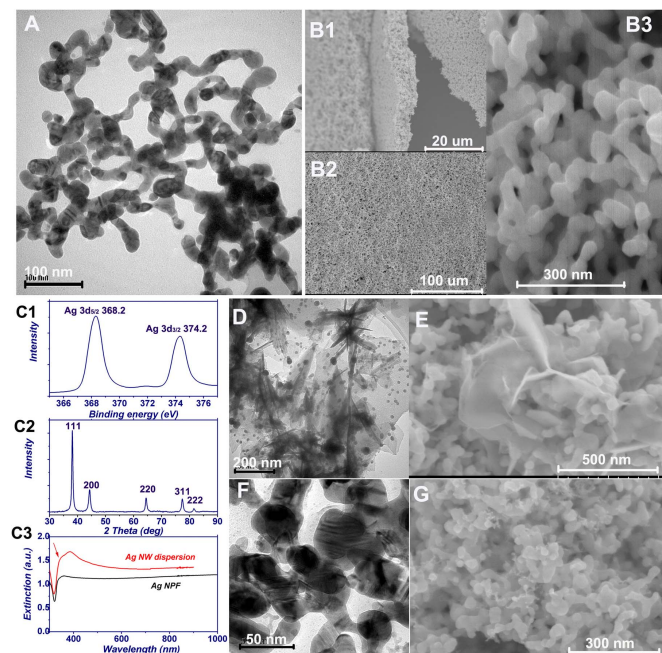

Fig.1 Morphological and spectroscopic characterization of fabricated nanostructures: (A) TEM images of Ag NWs; (B1-B3) FESEM image of Ag NPF at different magnifications; (C1-C3) XPS, XRD and UV-vis extinction spectra of Ag NWs and Ag NPF; TEM and FESEM image of Ag NPF-γ-Fe_2O_3 (D-E) and Ag@Pd NPF (F-G).

As illustrated in Fig. 1D and S2-3, after directly injecting $FeCl_3$ into the freshly synthesized Ag NWs, large areas of γ-Fe_2O_3 NSs were formed (Characterization and discussion of the synthesized γ-Fe_2O_3 NSs are presented in Fig. S3-4 in ESI).[10] Intriguingly, some nanoparticles with diameters of 20-50 nm were also present on the NSs. These particles were residual Ag NPs that did not connect into Ag NWs, and their adsorption on γ-Fe_2O_3 NSs could serve to provide an additional SERS substrate, thus facilitating the SERS detection of adsorbed As(III)/As(V) ions. After co-precipitation with Ag NWs, a uniform film was formed (Fig. 1E). Surprisingly, in the presence of γ-Fe_2O_3 NSs, the film displayed a light green colour, whereas the pure Ag NPF showed the characteristic colour of bulk Ag (Fig. S2). We attribute this to the constrained interconnection of Ag NWs by the incorporated γ-Fe_2O_3 NSs. Besides the metal oxide, a catalytic active transition metal, Pd, was also integrated into the Ag NPF, both in the form of an overlayer and NWs/branches (Fig. 1F-G and S5-6). The formation of an epitaxially grown Pd overlayer is supported by the presence of Moire patterns that arise from the superposition of misfited Pd and Ag crystalline lattices.[11] Besides the Pd overlayer, FESEM observation also revealed that some Pd NWs/branches anchored on Ag NWs were precipitated into Ag@Pd NPF.

The high extinction of Ag NPF in the vis/NIR range indicates that the Ag NPF would display high SERS activity under laser excitation at different wavelengths. Moreover, its 3D nanoporous structure may embody Raman hotspots such as nanopores/nanogaps, nanojunctions, and nanowells.[6d, 6f] Additionally, good uniformity of the NPF is important for generating reproducible SERS spectra. To demonstrate the SERS performance of Ag NPF, point-by-point Raman mapping

was performed on a randomly selected 400×400 μm^2 area on a Ag NPF loaded with 10^{-8} M thiophenol (TP) (step size of $5 \times 5 \mu m^2$, 6561 spectra). Fig. 2A shows the SERS intensity at 1077 cm^{-1}, attributed to the phenyl ring mode of TP, under laser excitation at 785 nm. The homogeneous distribution of the intense Raman signal strongly supports the notion that the Ag NPF is uniform over a large area and is capable of generating SERS signal with good reproducibility. Furthermore, the intensity distribution of the SERS peak at 1077 cm^{-1} excited at 785, 633 and 532 nm, and the corresponding relative standard deviations (RSD) of 13.4, 17.8 and 18.5%, again confirms the homogeneity of the Ag NPF (Fig. 2B, S9). It is worth noting that there is no apparent wavelength dependence of the Raman signal, since there is no change in relative intensity at different excitation wavelengths. This exceptional uniformity and fairly large enhancement of SERS signal make Ag NPF an ideal detection platform for single-molecule vibrational spectroscopy using low-cost SERS sensors.
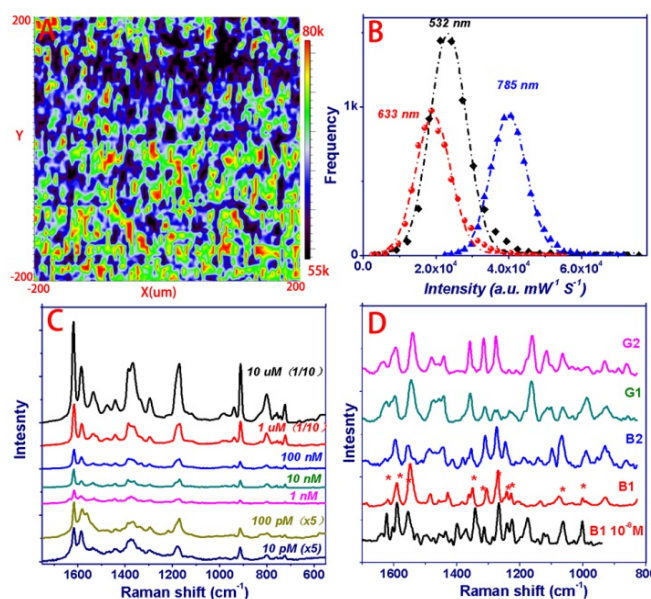

Fig. 2 (A, B) SERS mapping at 1077 cm^{-1} excited at 785 nm and intensity distribution under different excitation wavelengths. (C) Representative SERS spectra of CV at various concentrations, and (D) SERS spectra of 10^{-6} M AFTs and 10^{-8}M AFT B1.

The potential utilization of Ag NPFs in ultrasensitive SERS analysis was further corroborated *via* single molecule detection (SMD) of crystal violet (CV). As shown in Fig. 2C, well-discriminable SERS spectra are achieved for CV down to a concentration of 10^{-11} M, and the calculated enhancement factor reached 5.5×10^8 or above when excited at 532 or 633 nm. Furthermore, 25 out of 1000 spectra from a Ag NPF loaded with 10^{-13}M CV were identified as the SERS spectra of CV, again confirming the SMD capacity of Ag NPF (See discussion and Fig. S10-11 in ESI). Besides SMD for CV, high sensitivity was also demonstrated for analytes such as aflatoxins (AFTs),[12] which are toxic contaminants frequently found in crops and other foods. Because the structural resemblance of different AFTs results in spectral similarity, direct spectroscopic differentiation of AFT G_1, G_2, B_1, and B_2 based on their SERS spectra is challenging (10^{-6} M, described in Fig. 2D). The well-identifiable spectrum of B1 at very low concentrations (10^{-8} M) reveals the advantage of employing SERS in fast screening of AFTs.

Unlike Raman probes or pure chemicals found in the laboratory, samples for real-world applications are complicated to analyze by SERS due to very low concentrations of target analytes and potential

contamination with other chemicals. Therefore, selective enrichment of target analytes is of interest. For this purpose, we developed Ag NPFs doped with γ-Fe$_2$O$_3$ NSs that showed superior As(III)/As(V) ion capture performance.[10] We evaluated the ability of these fabricated Ag NPF-γ-Fe$_2$O$_3$ NSs to detect As(III)/As(V) ions from water samples. As(III)/As(V) ions were captured from water samples (5 mL) containing 10 μg L^{-1}As ion, which is the recommended maximum allowable value for drinking water as set by the WHO/USEPA. The captured ions were then analyzed by a portable Raman spectrometer (Enwave Optronics, Inc. USA). Besides the Raman peaks of γ-Fe$_2$O$_3$, i.e., 380, 460, and the broad peak at 1350 cm^{-1}, we observed new peaks from As-O at 796 cm^{-1} and 730 cm^{-1} for As(V) and As(III), respectively (Fig. 3A). The partial oxidation of As(III) is either attributed to γ-Fe$_2$O$_3$ induced chemical oxidation or photo-oxidation during SERS analysis. The feasibility of employing Ag NPF-γ-Fe$_2$O$_3$ NSs for quantitative SERS analysis of As(V) is further validated by the discriminable peak for 1.0 μg L^{-1} of As(V) and the linear relationship between As(V) concentration and the area of the peak at ~800 cm^{-1} (Fig. 3B-C).
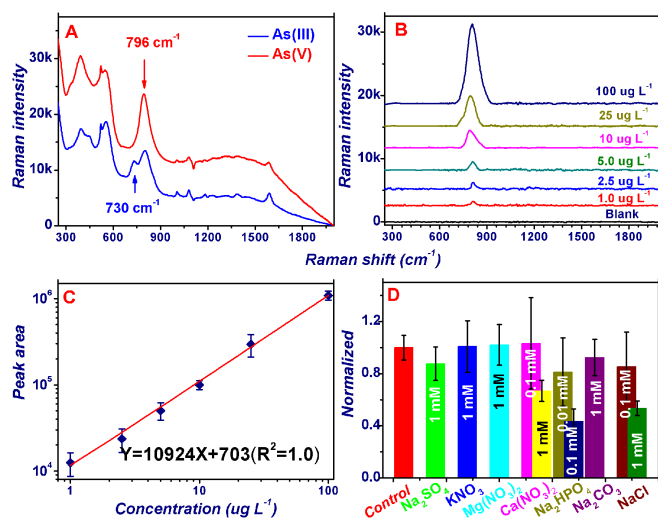
Fig. 3(A) SERS spectra of 10 μg L^{-1} As(III) and As(V) captured on Ag NPF-γ-Fe$_2$O$_3$ NSs; (B, C) background-subtracted SERS spectra of As(V) and the corresponding peak area as a function of concentration; (D) Tolerance of SERS detection of 7.5 μg L^{-1} or 0.1μM of As(V) to interference from co-existing ion on Ag NPF-γ-Fe$_2$O$_3$.

A series of experiments were performed to verify that As(III)/As(V) was adsorbed on γ-Fe$_2$O$_3$ and that the Ag surface was blocked by AgCl, as this determines the anti-interference capacity of the fabricated nanostructure.[13] A strong Cl$^-$ signal was observed on the Ag NPF-γ-Fe$_2$O$_3$ NSs (Fig. S4). Since γ-Fe$_2$O$_3$ did not adsorb Cl$^-$ (data not shown), and considering the high affinity of Ag for Cl$^-$, it is reasonable to assign the detected Cl$^-$ signal to the AgCl on the Ag surface. The existence of the AgCl layer is further supported by the following experiments. During the formation of Ag NPF, an equal amount of Cl$^-$ (0.6 mM) was added, and a strong Cl$^-$ signal was detected on the fabricated Ag NPF. However, no AgCl was observed in the corresponding XRD pattern (Fig S7), suggesting that the AgCl was present as thin layer on the Ag NPF surface. We also compared the SERS performance of three probe molecules, whose affinity for Ag is in the order of As(V) < SCN$^-$ < aminothiophenol (ABT), on Ag NPF (Cl) and Ag NPF. Of note, the existence of AgCl on Ag NPF has a negligible effect on the SERS activity of the Ag NPF, as is verified by the comparable signal intensity of the probe molecule CV (Fig.S14). The relationship between binding strength and SERS intensity indicated the presence of a AgCl layer on the Ag NPF(Cl): (i) only a small fraction of the total As(V) ions can be adsorbed onto

Ag NPF(Cl), resulting in ten-fold lower SERS intensity; (ii) some Cl$^-$ ions can be replaced by SCN$^-$, resulting in an increased SERS intensity that is still lower than that of Ag NPF; (iii) while for its strong binding with Ag and replacing the Ag-Cl bond with Ag-S or Ag-N, almost identical sensitivity was achieved for ABT (Fig.S15). Therefore, a AgCl layer does exist on Ag NPF, and its existence would constrain the direct adsorption of As(III)/As(V) ions onto Ag. The cooperation between SERS-active Ag NPF and As(III)-adsorbing γ-Fe$_2$O$_3$ is therefore the pivotal mechanism responsible for superior As ion detection. Meanwhile, SERS detection of As(III)/As(V) is largely unaffected by co-existing ions, with the exception of HPO$_4$$^{2-}$ (Fig. S16), an anion that has similar adsorption behavior as As(V) ion. Together, these data demonstrate successful fabrication of a SERS substrate for As(III)/As(V) detection (Fig. 3D).
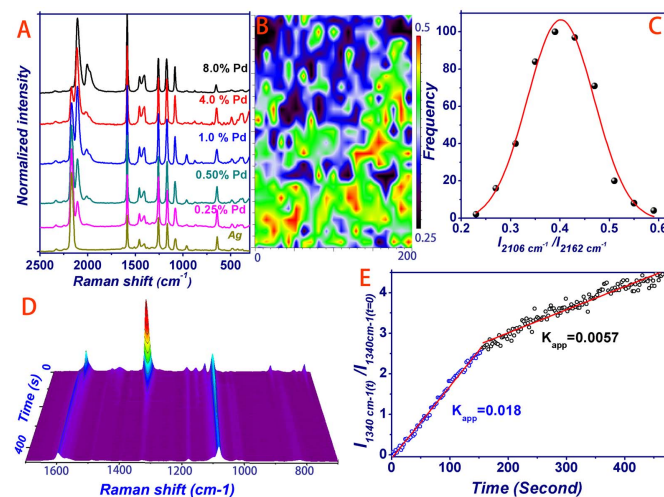
Fig. 4(A) Evolution of the SERS spectra of 2,6-DMPI with increasing amount of Pd; (B, C) Uniformity of Pd on Ag@Pd NPF as shown by SERS mapping; (D, E) 3D SERS mapping recorded on p-NTP-loaded Ag@Pd NPF (800 spectra, 0.5 s/spectrum), and calculation of the corresponding rate constant by a first-order reaction model.

In addition to its frequent application in analytical chemistry, SERS is becoming an important detection method in areas such as operando SERS monitoring of catalyzed reactions.[3d] To study the application of SERS for operando studies, Pd was deposited on a Ag surface, and its presence was verified by SERS detection of 2,6-dimethylphenylisocyanide (2,6-DMPI), whose potential in distinguishing the surface composition of bimetallic nanoarchitecture is well-acknowledged.[3d, 14] Fig. 4A illustrates the evolution of the SERS spectra with increasing amounts of Pd, where the peak at 2167 cm^{-1} is attributed to the 2,6-DMPI anchored on Ag atoms. This peak exhibited a red-shift to ~2110 or 2005/1970 cm^{-1} after binding to Pd atoms. The former peak was ascribed to atop bonded 2,6-DMPI, and the doublet peak near 2000 cm^{-1} was ascribed to the bridge-bound 2,6-DMPI. We tentatively assigned the peak at 2110 cm^{-1} to the Pd layer and the peak at 2000 cm^{-1} to Pd NWs/branches on Ag NWs (See ESI). The uniformity of Pd on Ag@Pd NPF is demonstrated by SERS mapping, and the ratio between 2167 and 2110 cm^{-1} was employed as an indicator (Fig. 4B-C). Uniform Pd distribution is of great importance for its utilization in reaction studies.

To evaluate the ability of this task-specific SERS substrate to monitor catalyzed reactions, we performed an operando study of Pd-catalyzed p-Nitrothiophenol (p-NTP) reduction. After being loaded with p-NTP, the Ag@Pd NPF-deposited SiO$_2$ slide was adhered to a lab-built reactor, and the enhanced Raman spectra were consecutively collected from the same location. The real-time 3D reaction trace is shown in Fig. 4D. Upon the addition of 0.2 mM

KBH$_4$, the predominant Raman features of *p*-NTP, ~1340 and ~1570 cm^{-1}, quickly decayed in the first 150 s and disappeared within 450 s, followed by the emergence of a new band at 1590 cm^{-1}. These results demonstrate how Ag@Pd NPFs may be used to monitor chemical processes *in situ*. Moreover, no SERS signal associated with 4,4'-dimercapto-azobenzene (DMAB), a plausible intermediate of this reaction, was observed. Fig. 4E shows the plots of -Ln($I_{1340(t)}/I_{1340(t=0)}$) as a function of reaction time, where $I_{1340(t)}$ represents the SERS intensity at 1340 cm^{-1} at different times. The reaction kinetics on Ag@Pd NPF can be divided into two stages, both of which are first-ordered. Furthermore, the difference in deduced kinetic constants signifies the existence of different active centres. The first/fast period is likely catalyzed by the Pd layer on Ag, whereas the slow period can be explained either by the transfer of *p*-NTP on the Ag surface to a nearby Pd atom and its reduction near the Pd atom,[3c, 3d] or conversion of *p*-NTP on Pd NWs/branches. However, most of the Ag surface was blocked by Pd, as shown in Fig. 4A, suggesting that the slow reaction occurred on the Pd NWs.

In conclusion, we developed a new method for the fabrication of Ag NPF as a SERS substrate from the self-deposition/organization of Ag NWs. The Ag NPF demonstrated favorable SERS performance when excited by both visible and NIR wavelengths, as seen in its large area uniformity and its successful performance in SMD of a dye molecule and high sensitivity detection of AFTs. Compared to other methods for SERS substrate fabrication, the proposed template-free procedure has numerous advantages, including low cost and ease of operation. Additionally, the prepared Ag NPFs showed high purity and porosity, large surface area, and small ligament diameter. Furthermore, because the Ag NPF fabrication process is compatible with co-sedimentation, we proposed and demonstrated the design of a group of new task-specific SERS substrates generated by co-precipitating nanomaterials such as nanosorbent and nanocatalyst into Ag NWs. The fabricated hybrid nanoarchitectures allowed us to perform ultra-sensitive SERS detection of As(V) ions with high tolerance for co-existing ions. We also conducted an operando survey of a catalyzed reaction. The reported method can be applied to plasmonic metal NWs such as ultrathin Au NWs and can also incorporate other materials into Au NPF (Fig. S17). In our laboratory, we are currently investigating the feasibility of incorporating living cells into biocompatible Au NPF for *in vivo* SERS monitoring of biological events at the single-cell level. Beyond SERS analysis and survey, the fabricated hierarchical nanoarchitecture may have promising applications in other surface plasmon resonance (SPR) related-fields, including SPR acceleration of chemical reactions.

Notes and references

a State Key Laboratory of Environmental Chemistry and Ecotoxicology, Research Center for Eco-Environmental Sciences, Chinese Academy of Sciences, Beijing 100085, China.jfliu@rcees.ac.cn.

b State Key Laboratory of Heavy Oil Processing and Department of Materials Science and Engineering, China University of Petroleum, Beijing 102249, China

1. (a) Y. J. Chen, W. P. Chen and E. Burstein, *Phys. Rev. Lett.*, 1976, **36**, 1207; (b) D. L. Jeanmaire and R. P. Vanduyne, *J. Electroanal. Chem.*, 1977, **84**, 1.
2. (a) S. M. Nie and S. R. Emery, *Science*, 1997, **275**, 1102; (b) N. P. W. Pieczonka and R. F. Aroca, *Chem. Soc. Rev.*, 2008, **37**, 946.
3. (a) X. D. Chen, A. B. Braunschweig, M. J. Wiester, S. Yeganeh, M. A. Ratner and C. A. Mirkin, *Angew. Chem. Int. Edit.*, 2009, **48**, 5178; (b) V. Joseph, C. Engelbrekt, J. D. Zhang, U. Gernert, J. Ulstrup and J. Kneipp, *Angew. Chem. Int. Edit.*, 2012, **51**, 7592; (c) J. F. Huang, Y. H. Zhu, M. Lin, Q. X. Wang, L. Zhao, Y. Yang, K. X. Yao and Y. Han, *J. Am. Chem. Soc.*, 2013, **135**, 8552; (d) R. Liu, J. F. Liu, Z. M. Zhang, L. Q. Zhang, J. F. Sun, M. T. Sun and G. B. Jiang, *J. Phys. Chem. Lett.*, 2014, **5**, 969.
4. (a) P. D. Howes, S. Rana and M. M. Stevens, *Chem. Soc. Rev.*, 2014, **43**, 3835; (b) B. Kang, M. M. Afifi, L. A. Austin and M. A. El-Sayed, *Acs Nano*, 2013, **7**, 7420; (c) D. Craig, S. McAughtrie, J. Simpson, C. McCraw, K. Faulds and D. Graham, *Anal. Chem.*, 2014, **86**, 4775; (d) L. L. Qu, D. W. Li, L. X. Qin, J. Mu, J. S. Fossey and Y. T. Long, *Anal. Chem.*, 2013, **85**, 9549; (e) S. P. Ravindranath, K. L. Henne, D. K. Thompson and J. Irudayaraj, *Acs Nano*, 2011, **5**, 4729.
5. (a) J. X. Fang, S. Y. Du, S. Lebedkin, Z. Y. Li, R. Kruk, M. Kappes and H. Hahn, *Nano Lett.*, 2010, **10**, 5006; (b) J. F. Li, Y. F. Huang, Y. Ding, Z. L. Yang, S. B. Li, X. S. Zhou, F. R. Fan, W. Zhang, Z. Y. Zhou, D. Y. Wu, B. Ren, Z. L. Wang and Z. Q. Tian, *Nature*, 2010, **464**, 392; (c) M. Chirumamilla, A. Toma, A. Gopalakrishnan, G. Das, R. P. Zaccaria, R. Krahne, E. Rondanina, M. Leoncini, C. Liberale, F. De Angelis and E. Di Fabrizio, *Adv. Mater.*, 2014, **26**, 2353.
6. (a) H. L. Liu, Z. L. Yang, L. Y. Meng, Y. D. Sun, J. Wang, L. B. Yang, J. H. Liu and Z. Q. Tian, *J. Am. Chem. Soc.*, 2014, **136**, 5332; (b) M. Rycenga, C. M. Cobley, J. Zeng, W. Y. Li, C. H. Moran, Q. Zhang, D. Qin and Y. N. Xia, *Chem. Rev.*, 2011, **111**, 3669; (c) K. L. Wustholz, A. I. Henry, J. M. McMahon, R. G. Freeman, N. Valley, M. E. Piotti, M. J. Natan, G. C. Schatz and R. P. Van Duyne, *J. Am. Chem. Soc.*, 2010, **132**, 10903; (d) R. Liu, J. F. Liu, X. X. Zhou, M. T. Sun and G. B. Jiang, *Anal Chem*, 2011, **83**, 9131; (e) Y. Bao, C. L. Lai, Z. T. Zhu, H. Fang and C. Y. Jing, *RSC Adv.*, 2013, **3**, 8998; (f) L. H. Qian, X. Q. Yan, T. Fujita, A. Inoue and M. W. Chen, *Appl Phys Lett*, 2007, **90**, 153120.
7. Y. Fang, N. H. Seong and D. D. Dlott, *Science*, 2008, **321**, 388.
8. (a) G. Lu, H. Li, C. Liusman, Z. Y. Yin, S. X. Wu and H. Zhang, *Chem. Sci.*, 2011, **2**, 1817; (b) W. Ren, Y. X. Fang and E. K. Wang, *Acs Nano*, 2011, **5**, 6425; (c) K. Jasuja and V. Berry, *Acs Nano*, 2009, **3**, 2358.
9. R. Liu, J. F. Liu and G. B. Jiang, *Chem Commun*, 2010, **46**, 7010.
10. R. Liu, J. F. Liu, L. Q. Zhang, J. F. Sun, Z. M. Zhang and G. B. Jiang, *Submitted*.
11. F. R. Fan, D. Y. Liu, Y. F. Wu, S. Duan, Z. X. Xie, Z. Y. Jiang and Z. Q. Tian, *J. Am. Chem. Soc.*, 2008, **130**, 6949.
12. (a) K. M. Lee, T. J. Herrman, Y. Bisrat and S. C. Murray, *J. Agr. Food. Chem.*, 2014, **62**, 4466; (b) A. M. Moricz, E. Horvath, P. G. Ott and E. Tyihak, *J. Raman. Spectrosc.*, 2008, **39**, 1332.
13. (a) Z. H. Xu, J. M. Hao, F. S. Li and X. G. Meng, *J. Colloid. Interf. Sci.*, 2010, **347**, 90; (b) J. J. Du, J. L. Cui and C. Y. Jing, *Chem. Commun.*, 2014, **50**, 347.
14. S. M. Gruenbaum, M. H. Henney, S. Kumar and S. Z. Zou, *J. Phys. Chem. B*, 2006, **110**, 4782.

ChemComm Accepted Manuscript